Finite Element Modeling of Acoustic Singularities with Application to Propeller Noise

W. Eversman* and J. E. Steck†
University of Missouri, Rolla, Missouri

Numerical formulations and results that expand on recent developments in finite element modeling of acoustic volume sources and acoustic dipoles are presented. It is shown that with a suitable structuring of the acoustic field equations it is possible to include monopoles and dipoles within the same analysis framework as has been extensively used for interior duct acoustic and duct inlet radiation problems. This allows the extension of the finite element modeling method to include the noise sources in such applications as propellers enclosed in a duct or in free space with mean flows. The necessary structuring of the acoustic field equations is shown, and example calculations are given for the case of one-dimensional sources and body forces in the presence of mean flow, two-dimensional sources, axial body forces, and transverse body forces in the presence of uniform mean flow. Three-dimensional sources and dipoles are modeled as the Fourier sum of axially symmetric solutions without the necessity of introducing "singular elements." It is further demonstrated that distributions of singularities can be readily modeled, and an example is given of the computation of the near- and far-field radiation of a propeller. Comparison of the far-field radiation directivity is made with the Gutin theory.

Introduction

FINITE element methods have proved to be effective for solving field equations in a variety of applications in aeroacoustics. Included in recent developments have been modeling of the acoustic transmission in ducts without mean flow,[1] transmission in ducts with a nonuniform mean flow,[2] and radiation from duct inlets without[3] and with[4,5] mean flow. These applications have been supported by studies of the fundamental characteristics of the solution methods employed.[6,7] Efficient computer programs using rapid access external disk storage and frontal solution methods[8] have been developed. These programs can handle physically realistic duct transmission and radiation problems with storage requirements well within the capability of most mainframe computer systems and even within the capability of many smaller "distributed processing"-type systems. In terms of the capabilities of "supercomputers," the computational requirements are relatively small.

In the applications noted above, both interior and exterior types of acoustic propagation problems have been addressed. In the interior problems,[1,2] the solution domain was closed by imposing boundary conditions on a modal basis describing a known reflection (or lack of reflection) or known generating mechanism at a boundary. In the exterior problems,[3-5] the region was closed in the far field by imposing a suitable representation of a radiation condition with the aid of special "infinite" or "wave envelope" elements to bridge the gap between the near and far field with a minimum of mesh refinement.

These duct transmission and radiation examples are characterized by an imprecise knowledge of the noise-generating mechanism. The only knowledge assumed is the modal characteristics in terms of modal amplitudes presumably provided from measurements but almost certainly not from theoretical noise source models. This is not to imply that techniques of noise source modeling are not known. In the propeller noise problem in the free field, source modeling has been attempted since the 1930s (the Gutin theory[9] being the notable example) and has been developed to a high degree of sophistication in recent years, chiefly by Farassat[10] and Hanson.[11] The acoustic analogy used in the propeller theories is equally applicable in the ducted rotor or rotor stator situation. Indeed, Clark et al.[12] produced a considerable theory and computer code for this purpose. The more substantial development of the propeller noise theories stems from the manner in which the acoustic analogy is implemented through fundamental solutions for volume sources and dipoles in a free field. Fundamental solutions for sources and dipoles in the interior of a duct, with radiation permitted to the far field, are not possible to obtain analytically, except in simple cases.

In this paper a direct numerical approach to the acoustic analogy is explored, with emphasis on using this modeling method to represent complex noise-generating mechanisms. The first step in the study involves the extension of the previously developed finite element modeling techniques to problems involving the acoustic field equations with sources and body forces. For point sources and forces, solutions are in effect numerical fundamental solutions or "Green's functions" without the limitations imposed by requiring free-field or other simple boundary conditions. The boundary conditions and ambient state are an intrinsic part of the acoustic field representation.

Current propeller theories superpose the fundamental solutions via integral representations to obtain a noise source model. A fully numerical technique represents the extended noise source by a spatial distribution of source and body forces. The computation of the radiated acoustic field is no more difficult than the representation of the fundamental solutions for isolated singularities. In fact, it is less demanding because continuous source and force distributions replace the singularities.

The following sections demonstrate the success with which acoustic singularities can be modeled with finite element methods. Beginning with the acoustic field equations containing source and body force terms, and written to include the presence of a uniform mean flow, test cases are presented for which analytic solutions are readily available. The finite element formalism is introduced and it is shown that, with a simple interpretation of divergence terms in the field equations, the source and body force terms enter the solution process on

Presented as Paper 84-2286 at the AIAA/NASA 9th Aeroacoustics Conference, Williamsburg, VA, Oct. 15-17, 1984; received Jan. 18, 1985; revision received Oct. 10, 1985.

*Curators' Professor, Department of Mechanical and Aerospace Engineering. Associate Fellow AIAA.

†Graduate Student, Department of Mechanical and Aerospace Engineering. Member AIAA.

an equal footing without the necessity of directly handling spatial derivatives of point functions.

Following the statement of the finite element approximations, a comparison of exact and finite element solutions for one- and two-dimensional sources and dipoles is given. The two-dimensional examples are of singularities in a duct with reflection-free terminations. Three-dimensional comparison calculations are given for the specific example of a dipole off the axis of symmetry, directed along this axis and radiating to free space. The modeling method introduced here involves decomposing the solution into Fourier components, or angular modes, with respect to the axis of symmetry. This is consistent with the current duct propagation and radiation theories.

An example of a distributed source is provided by the Gutin propeller theory.[9] Finite element calculations are shown for the near- and far-field acoustic radiation and directivity of a two-bladed propeller. The Gutin theory is used to provide a baseline against which the directivity results can be compared.

Acoustic Sources and Dipoles in Uniform Flow

Preparatory to consideration of the use of a finite element method for the solution of problems in propeller noise generation and propagation, it is appropriate to consider the more elementary problem of modeling acoustic sources and dipoles. These simple singularities are of central importance in describing more complex noise sources using the acoustic analogy.

The governing equation for acoustic sources and dipoles in a uniform flowfield is the nondimensional acoustic wave equation:

$$\nabla^2 p - \left[\frac{\partial}{\partial t} + M\frac{\partial}{\partial x}\right]^2 p = \nabla\cdot\vec{f} - \left[\frac{\partial}{\partial t} + M\frac{\partial}{\partial x}\right] q \tag{1}$$

A somewhat altered form of Eq. (1) is more useful in the finite element formulation in that divergence terms have particular significance. This form is

$$\nabla^2 p - \left[\frac{\partial}{\partial t} + M\frac{\partial}{\partial x}\right]^2 p = \nabla\cdot\vec{f} - \nabla\cdot\vec{M}q - \frac{\partial q}{\partial t} \tag{2}$$

noting that $\vec{M} = M\vec{i}$ and M is a constant over the domain. For a harmonically varying body force and source with a time dependence of the form $\exp(i\eta_r t)$, the convected wave equation becomes

$$\nabla^2 p - \left[i\eta_r + M\frac{\partial}{\partial x}\right]^2 p = \nabla\cdot\vec{f} - \nabla\cdot\vec{M}q - i\eta_r q \tag{3}$$

$$\eta_r = \omega L/c \tag{4}$$

In Eqs. (1-4) pressure is nondimensionalized by ρc^2, velocity by c, and lengths by a suitable reference length L.

Finite Element Formulation

A standard weighted residual method is used to establish the finite element formulation of Eqs. (2) and (3). This involves multiplying Eq. (3) by an arbitrary weighting function W_i and integrating over the problem domain. It can be shown that a solution of Eq. (3) is also a solution of the following weighted residual statement.

Find a function p, such that

$$\int_\Omega W_i\left[\nabla\cdot\left(\nabla p - M^2\frac{\partial p}{\partial x}\vec{i} - \vec{f} + \vec{M}q\right) - 2i\eta_r M\frac{\partial p}{\partial x} + \eta_r^2 p + i\eta_r q\right] d\Omega + \int_{\partial\Omega} W_i\left[\left(\nabla\bar{p} - M^2\frac{\partial\bar{p}}{\partial x}\vec{i}\right) - \left(\nabla p - M^2\frac{\partial p}{\partial x}\vec{i}\right)\right]\cdot\vec{n}\,dS = 0 \tag{5}$$

for all trial functions W_i of a suitable set of functions.[13] Ω is the solution domain and $\partial\Omega$ the surface bounding Ω on which $\vec{n}$ is the outward normal unit vector. The volume integral is the weighted residual of the field equation. The surface integral is the weighted residual of the boundary condition. If the divergence theorem is used and if $\vec{f}$ and q are zero on the outer boundary of the domain, then Eq. (5) can be written as

$$\int_\Omega \left[\nabla W_i\cdot\left(\nabla p - M^2\frac{\partial p}{\partial x}\vec{i} - \vec{f} + \vec{M}q\right) + 2i\eta_r M W_i\frac{\partial P}{\partial x} - \eta_r^2 W_i p - i\eta_r W_i q\right] d\Omega - \int_{\partial\Omega} W_i\left[\left(\nabla\bar{p} - M^2\frac{\partial\bar{p}}{\partial x}\vec{i}\right)\right]\cdot\vec{n}\,dS = 0 \tag{6}$$

The Galerkin finite element approximation of Eq. (6), in general, involves dividing the problem domain into many finite subdomains, called finite elements. For each element, interpolation node points are chosen. The unknown pressure function, p, and the arbitrary weighting function, W_i, are approximated on each element by interpolation functions. The interpolation function for the pressure is written entirely in terms of the unknown values of the function p at the nodes of each element; similarly for the weight function W_i. Since the weight function is arbitrary, and thus its nodal values are arbitrary, this approximation of Eq. (6) yields a system of linear algebraic equations that can be solved for the unknown nodal pressures. Several cases will now be considered to demonstrate the results of the finite element modeling of sources and dipoles.

An Acoustic Source in One Dimension with Reflection-Free Boundaries

In one dimension, Eq. (3) becomes

$$(1-M^2)\frac{d^2p}{dx^2} - 2i\eta_r M\frac{dp}{dx} + \eta_r^2 p = \frac{df_x}{dx} - M\frac{dq}{dx} - i\eta_r q \tag{7}$$

and the weighted residual statement from Eq. (6) is

$$\int_{-1}^{1}\left[(1-M^2)\frac{dW_i}{dx}\frac{dp}{dx} - \frac{dW_i}{dx}(f_x - Mq) + 2i\eta_r M W_i\frac{dp}{dx} - \eta_r^2 W_i p - i\eta_r W_i q\right] dx + \int_{-1}^{1} W_i\left[i\left(\frac{\eta_r}{1-M}\right)(1-M^2)p(x=-1)\delta(x+1) + i\left(\frac{\eta_r}{1+M}\right)(1-M^2)p(x=1)\delta(x-1)\right] dx = 0 \tag{8}$$

The boundary terms in Eq. (8) represent the reflection-free condition at $x=1$ and -1 described by

$$\frac{dp}{dx} = -i\left(\frac{\eta_r}{1+M}\right)p, \qquad x=1$$

$$\frac{dp}{dx} = i\left(\frac{\eta_r}{1+M}\right)p, \qquad x=-1 \tag{9}$$

Equations (7-9) describe the propagation of plane waves in an infinite tube containing a mean flow with volume sources and body forces.

Equation (8) is used as the weak problem from which a Galerkin finite element formulation is obtained using three-

noded quadratic elements.[14] The acoustic pressure field is written in terms of the global shape function matrix $[N(x)]$, which interpolates the pressure $p(x)$ using the vector of nodal values $\{p\}$ according to $p(x)=[N(x)]\{p\}$. The weighting functions W_i are interpolated by the shape functions in the row matrix $[N(x)]$. Equation (7) is then approximated by the matrix problem

$$\left[\int_{-1}^{1}\{(1-M^2)[N_x]^T[N_x]+2i\eta_r M[N]^T[N_x] - \eta_r^2[N]^T[N]\}dx\right]\{p\}+[BC]\{p\} = \int_{-1}^{1}\{[N_x]^T[f_x(x)-Mq(x)]+i\eta_r[N]^Tq(x)\}dx \quad (10)$$

where

$$[BC]=i\eta_r(1+M)[N(-1)]^T[N(-1)] + i\eta_r(1-M)[N(1)]^T[N(1)] \quad (11)$$

is a square diagonal matrix with nonzero elements corresponding only to the nodal values of pressure at $x=1$ and -1. Note also that because of the significance of the shape and weighting functions, the two matrix operations yield square matrices with only a single term of unity corresponding to the nodal pressures at $x=1$ and -1.

In terms of a global "stiffness" matrix $[K]$, and a global "force" or data vector $\{f\}$, Eq. (10) becomes

$$[K]\{p\}=\{f\} \quad (12)$$

where

$$[K]=\int_{-1}^{1}\{(1-M^2)[N_x]^T[N_x]+2i\eta_r[N]^T[N_x] - \eta_r^2[N]^T[N]\}dx+[BC] \quad (13)$$

and

$$\{f\}\int_{-1}^{1}\{[N_x]^T(f_x(x)-M_q(x))+i\eta_r[N]^Tq(x)\}dx \quad (14)$$

The stiffness matrix and force vector are generated by explicitly defining the shape matrix within each element, carrying out the indicated operations element by element, and assembling according to standard procedures.[15]

An acoustic source located at $x=0$ is defined by

$$q(x)=Q\delta(x) \quad (15)$$

where Q is the volumetric source strength. The force vector, with zero body force, is

$$\{f\}=Q\int_{-1}^{1}\{i\eta_r[N]^T-M[N_x]^T\}\delta(x)dx \quad (16)$$

This integral has only a contribution within the element containing the source. The element force vector for the source is written as

$$\{f\}_s^e=Q\{i\eta_r[N^e(0)]^T-\frac{2}{\Delta}M[N_\xi^e(0)]^T\} \quad (17)$$

where $[N^e(0)]$ and $[N_\xi^e(0)]$ are the element shape marix and its derivative with respect to ξ evaluated at $\xi=0$ on the interval $-1\le\xi\le1$. A three-noded parent line element is used. The element in the global x coordinate system is of length Δ and the source is at the center node of the element. The element force vector described by Eq. (17) is the 3×1 column vector

$$\{f\}_s^e=Q\left[\frac{M}{\Delta},\ i\eta_r,\ -\frac{M}{\Delta}\right]^T \quad (18)$$

A word is appropriate here regarding the decision to place the acoustic singularity at the midpoint of the element. An acoustic source will cause a discontinuity in both acoustic pressure and pressure derivative. In the present development, no effort has been made to construct special singular elements. The elements used here to interpolate the pressure solution force the numerical solution to be continuous interior to the elements, but they allow pressure slope discontinuities at element boundaries. When such elements are used to approximate the functions of the weak problem of Eq. (8), it is not possible to duplicate the singular (Dirac delta) nature of the source in Eq. (15) exactly. The placement of the source at an interior node implies that the Dirac delta is introduced in approximation only as a continuous interpolation function formed by the shape functions on the element containing the source. As long as the elements are made relatively small near the source, the effect of this approximation is limited to altering the solution only in the region near the source.

The exact solution for a unit source at $x=0$ with reflection-free boundaries is

$$p=\frac{1}{2}\frac{1}{1+M}\exp\left[-\frac{i\eta_r}{1+M}x\right], \quad x>0 \quad (19)$$

$$p=\frac{1}{2}\frac{1}{1-M}\exp\left[\frac{i\eta_r}{1-M}x\right], \quad x<0 \quad (20)$$

The accuracy with which the finite element method can represent this singularity is shown in Figs. 1 and 2. These figures are for a unit source at $x=0$ at a Mach number of $M=-0.3$. This is a flow directed toward the source in the $-x$ direction. Forty-one 3-noded quadratic elements are used to approximate the domain, $-1<x<1$, with the source in the center of the middle element. Reflection-free boundaries are simulated at both ends, $x=1$ and -1. Dimensionless frequencies, kL, which produce wavelengths of $(1+M)(\lambda L)=10(\Delta/L)$ and $4(\Delta/L)$ on the upstream side are $kL=9.0$ and 22.5. Computations were made for this range of convected wavelengths. Computations with four elements per wavelength are expected to be only marginally adequate.

Figures 1 and 2 show the comparisons between the exact solution and the finite element solutions for the case of 10 elements per wavelength upstream. It is seen that, except for near the source, the finite element representation is nearly exact. Somewhat degraded, but acceptable results are obtained with as few as four elements per wavelength upstream. These results are consistent with the usual supposition that quadratic elements require four to six elements per wavelength for acceptable accuracy.

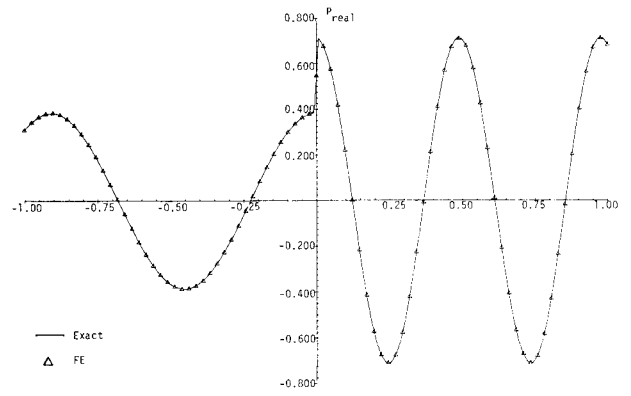

Fig. 1 Real part of pressure for one-dimensional point source at $x=0.0$, $k=9.0$, 41 elements, $M=-0.3$. (FE = finite element.)

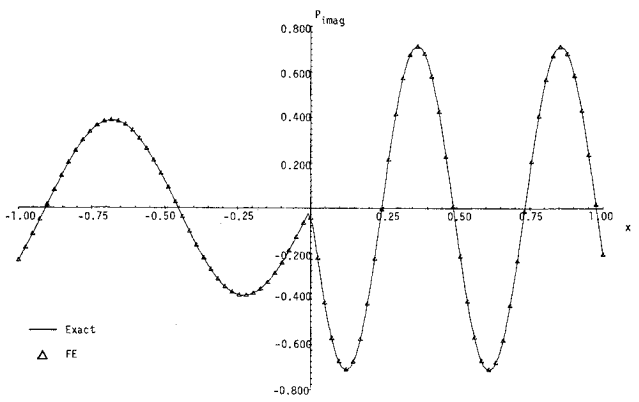

Fig. 2 Imaginary part of pressure for one-dimensional point source at $x=0.0$, $k=9.0$, 41 elements, $M=-0.3$. (FE = finite element.)

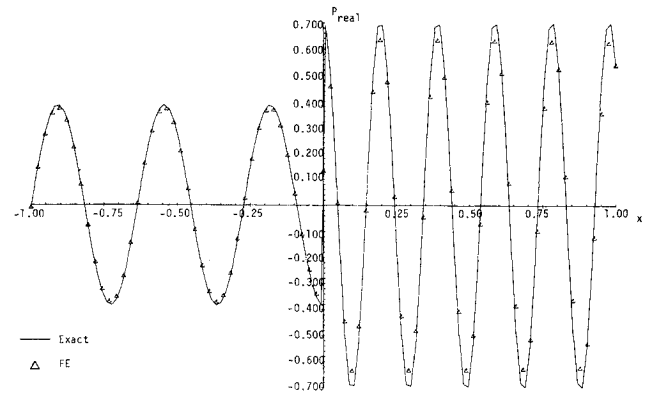

Fig. 3 Real part of pressure for one-dimensional point force at $x=0.0$, $k=22.5$, 41 elements, $M=-0.3$. (FE = finite element.)

The Acoustic Dipole in One Dimension with Reflection-Free Boundaries

An acoustic dipole at $x=0$ is defined by $f_x(x)=F\delta(x)$, where F is the force in the x direction, applied at $x=0$. In this case, the force vector in the absence of acoustic sources is

$$\{f\}=\int_{-1}^{1}[N_x]^T f_x(x)\,\mathrm{d}x$$

As in the case of the source, this integral has a contribution only within the element containing the dipole. In terms of the parent element coordinate ξ, $\xi\in[-1,1]$, the source element force vector is given by

$$\{f\}_s^e=\frac{2F}{\Delta}\,[N_\xi(0)]^T$$

This produces the 3×1 vector

$$\{f\}_s^e=F\left[\frac{-1}{\Delta},\ 0,\ \frac{1}{\Delta}\right]^T \tag{21}$$

The exact solution for a unit force in the x direction, at $x=0$, is

$$p=\frac{1}{2}\,\frac{1}{1+M}\exp\left[-\frac{i\eta_r}{1+M}x\right],\qquad x>0 \tag{22}$$

$$p=-\frac{1}{2}\,\frac{1}{1-M}\exp\left[\frac{i\eta_r}{1-M}x\right],\qquad x<0 \tag{23}$$

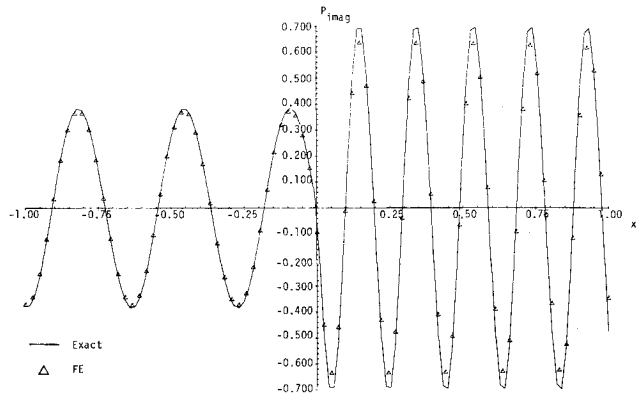

Fig. 4 Imaginary part of pressure for one-dimensional point force at $x=0.0$, $k=22.5$, 41 elements, $M=-0.3$. (FE = finite element.)

The accuracy with which the finite element method reproduces this result is shown in Figs. 3 and 4. The conditions are the same as those used to test the source solution in the previous section, except in this case we display the result for four elements per wavelength upstream. Even with this marginal resolution relatively good reproduction of the exact solution is achieved.

The Acoustic Source and Dipole in a Two-Dimensional Duct with Reflection-Free Terminations

In a two-dimensional duct, Eq. (3) becomes

$$(1-M^2)\frac{\partial^2 p}{\partial x^2}+\frac{\partial^2 p}{\partial y^2}-2i\eta_r M\frac{\partial p}{\partial x}+\eta_r{}^2 p$$

$$=\frac{\partial f_x}{\partial x}+\frac{\partial f_y}{\partial y}-M\frac{\partial q}{\partial x}-i\eta_r q \tag{24}$$

and the weighted residual statement from Eq. (6) is

$$\int_0^a\int_0^1\left[(1-M^2)\frac{\partial W_i}{\partial x}\frac{\partial p}{\partial x}+\frac{\partial W_i}{\partial y}\frac{\partial p}{\partial y}\right.$$

$$-\frac{\partial W_i}{\partial x}(f_x-Mq)-\frac{\partial W_i}{\partial y}f_y+2i\eta_r MW_i\frac{\partial P}{\partial x}$$

$$\left.-\eta_r^2 W_i p-i\eta_r W_i q\right]\mathrm{d}y\,\mathrm{d}x$$

$$+\left[\int_0^1(1-M^2)W_i\frac{\partial p}{\partial x}\,\mathrm{d}y\right]_{x=0}$$

$$-\left[\int_0^1(1-M^2)W_i\frac{\partial p}{\partial x}\mathrm{d}y\right]_{x=a}=0 \tag{25}$$

The reflection-free boundary condition at $x=0$ and a is achieved by representing the pressure at each end as a Fourier series in the variable y of the form

$$p=\sum_{i=1}^{N}C_n\exp(-ik_{x_n})\cos(n\pi y)$$

Specifically at each end,

$$p=\sum_{i=1}^{N}a_n\cos(n\pi y)\qquad\text{at } x=0 \tag{26}$$

$$p=\sum_{i=1}^{N}b_n\cos(n\pi y)\qquad\text{at } x=a \tag{27}$$

$$\frac{\partial p}{\partial x} = \sum_{i=1}^{N} (-ik_{x_n}^{-}) a_n \cos(n\pi y) \qquad \text{at } x=0 \tag{28}$$

$$\frac{\partial p}{\partial x} = \sum_{i=1}^{N} (-ik_{x_n}^{+}) b_n \cos(n\pi y) \qquad \text{at } x=a \tag{29}$$

where

$$\frac{k_{x_n}^{\pm}}{\eta_r} = \frac{1}{1-M^2}\left[-M \pm \sqrt{1-(1-M^2)\left(\frac{n\pi}{\eta_r}\right)^2}\right] \tag{30}$$

and the sign choice for positive and negative propagating or cutoff modes is determined by an energy argument.[16]

Again, following a standard Galerkin scheme, the matrix relationship

$$[K_T]\,[a,p,b]^T = \{f_T\} \tag{31}$$

is formed so that

$$[K_T] = \int_0^a \int_0^1 \{(1-M^2)[N_x]^T[N_x] + [N_y]^T[N_y] + 2i\eta_r[N]^T[N_x] - \eta_r^2[N]^T[N]\}\,dy\,dx + \int_0^1 (1-M^2)[N]^T[M^-]\,dy - \int_0^1 (1-M^2)[N]^T[M^+]\,dy \tag{32}$$

The terms a and b in Eq. (31) are vectors of the unknown Fourier coefficients of Eqs. (26) and (27). The "stiffness" matrix has degrees of freedom corresponding to these modal coefficients at the two ends and the pressures at all of the nodes. The modal matrices $[M^-]$ and $[M^+]$ are derived from Eqs. (28) and (29). The force vector is given by

$$\{f_T\} = [0, f, 0]^T \tag{33}$$

where

$$\{f\} = \int_0^a \int_0^1 \{[N_x]^T(f_x - Mq) + [N_y]^T f_y + i\eta_r[N]^T q\}\,dy\,dx \tag{34}$$

and corresponds only to nodal degrees of freedom. The final boundary condition [at $x=0$ and a, Eqs. (26) and (27), must be satisfied] can be imposed by using these relations as transformation matrices to "compress" the "stiffness" matrix by expressing the modal pressures on $x=0$ and a in terms of the modal coefficients a_n and b_n. This procedure is discussed in more detail by Eversman et al.[4] The integrations are carried out element by element and assembled by standard procedures.[14]

In the present study, the two-dimensional duct has been represented by a mesh of nine-noded Lagrangian elements related to a nine-noded parent element. The sources and body forces are applied at a point at the center of an element, again implying that the Dirac delta function is approximated by the continuous function generated by the shape functions. The element force vector for this element is then obtained from Eq. (34) as

$$\{f\}_s^e = \frac{2F_x}{\Delta x}[N_\xi(0)]^T + \frac{2F_y}{\Delta y}[N_\eta(0)]^T + Q\left(i\eta_r[N(0)]^T - \frac{2M}{\Delta x}[N_\xi(0)]^T\right) \tag{35}$$

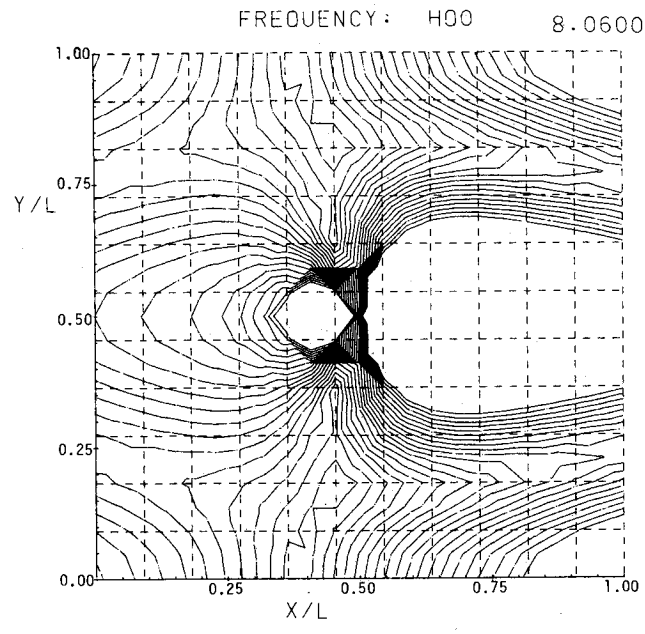

Fig. 5 Contours of equal pressure amplitude for an axial force at $x=0.50$, $y=0.50$, $kL=8.06$, $M=-0.3$.

where F_x and F_y are the point force magnitudes, Q the source strength, and Δx and Δy the x and y dimensions of the element. This nine-component vector, Eq. (35), is determined from the shape functions to be

$$\{f\}_s^e = F_x\left[0,0,0,0,0,\frac{-1}{\Delta x},\frac{1}{\Delta x},0,0\right]^T + F_y\left[0,0,0,0,\frac{-1}{\Delta y},0,0,\frac{1}{\Delta y},0\right]^T + Q\left[0,0,0,0,0,\frac{M}{\Delta x},\frac{-M}{\Delta x},0,i\eta_r\right]^T \tag{36}$$

The three vectors that combine to define the element force vector correspond to the x force component, y force component, and the source.

The exact solution for a unit force in the x direction located at $x=x_0$, $y=0.50$, in a duct of unit height is

$$P(x,y) = \frac{1}{1-M^2}\sum_n \frac{\cos(n\pi/2)}{N_{nn}}\frac{k_{x_n}^{+}}{(k_{x_n}^{+}-k_{x_n}^{-})} \times \cos(n\pi y)\exp[-ik_{x_n}^{+}(x-x_0)], \qquad x>0 \tag{37}$$

and

$$P(x,y) = \frac{1}{1-M^2}\sum_n \frac{\cos(n\pi/2)}{N_{nn}}\frac{k_{x_n}^{-}}{(k_{x_n}^{+}-k_{x_n}^{-})} \times \cos(n\pi y)\quad \exp[-ik_{x_n}^{-}(x-x_0)], \qquad x<0 \tag{38}$$

Comparisons between exact and finite element solutions for the axial force at $M=-0.3$ and $\eta_r=8.06$ are shown in Figs. 5-7. Figure 5 is the finite element result for equal pressure magnitude contours, and Figs. 6 and 7 show the real and imaginary parts of the acoustic pressure on the duct axis.

The Acoustic Dipole in Cylindrical Coordinates

Many problems of interest, including computation of the acoustic field of a propeller or radiation of fan noise, involve an axially symmetric geometry. In situations of this type, a cylindrical coordinate system is appropriate. Furthermore, the noise source is periodic in the angular coordinate and can be represented in terms of spinning Fourier modes with time and angular dependence, $\exp[i(\eta_r t - m\theta)]$. The Galerkin formulation of Eq. (6) in three dimensions can be reduced to a two-dimensional problem in the variables x (axial coordinate) and r (radial coordinate) by representing the functions p, W_i, q, and $\vec{f}$ of Eq. (6) as a complex Fourier series in the variable θ. For the function p,

$$p(r,\theta,x) = \sum_{M=-\infty}^{\infty} p_m(r,x)\exp(-im\theta) \tag{39}$$

where it has been previously assumed that $p(r,\theta,x,t) = p(r,\theta,x)\exp(i\eta_r t)$. Making these substitutions, where $d\Omega$ in Eq. (6) becomes $r\,dr\,d\theta\,dz$, and carrying out the integration over θ exactly gives,

$$2\pi \int_S \left[\nabla W_i \cdot \left(\nabla p_m - M^2 \frac{\partial p_m}{\partial x} \vec{i} - \vec{f}_m + \vec{M} q_m \right) + 2i\eta_r M W_i \frac{\partial p_m}{\partial x} - \eta_r^2 W_i p_m - i\eta_r W_i q_m \right] r\,dr\,dx - 2\pi \int_C W_i \left[\nabla \bar{p}_m - M^2 \frac{\partial \bar{p}_m}{\partial x} \vec{i} \right] \cdot \vec{n}\,ds = 0 \tag{40}$$

where W_{i_m} is written simply as W_i since the weight functions are arbitrary. S is the region in the x,r plane where $r \geq 0$, and is bounded by the far-field boundary curve, C. C has a differential arc length, ds, and a unit outward normal $\vec{n}$. The gradient operator is

$$\nabla = \frac{\partial}{\partial x}\vec{i} + \frac{\partial}{\partial r}\vec{e}_r - \frac{im}{r}\vec{e}_\theta \tag{41}$$

Equation (40) is simplified by assuming no flow or $M = 0$. The boundary curve is chosen to be a semicircle whose radius is many wavelengths of the noise sources, which are located near the origin. This allows simple implementation of a far-field or outgoing wave boundary condition on C as

$$\frac{\partial \bar{p}_m}{\partial n} = \frac{\partial \bar{p}_m}{\partial R} = \left[-i\eta_r - \frac{1}{R} \right] \bar{p} \text{ on } C \tag{42}$$

where $R^2 = r^2 + x^2$. For large R, $\frac{1}{2} \approx 0$.

Equation (40) is a two-dimensional equation. As such, it is approximated by a finite element scheme in the same manner as the previous two-dimensional problem of Eqs. (31-36) by using the nine-noded master element shape functions. This gives a stiffness matrix, for $M = 0$, of

$$[K] = \int_S \left([N_x]^T[N_x] + [N_r]^T[N_r] - \left(\eta_r^2 - \frac{m^2}{r^2} \right) [N]^T[N] \right) r\,dr\,dx + i\eta_r \int_C [N]^T[N]\,ds \tag{43}$$

The force or data vector is given by

$$\{f\} = \int_S \left([N_x]^T[N]\{F_{x_m}\} + i\frac{m}{r}[N]^T\{F_{\theta_m}\} + i\eta_r[N]^T\{Q_m\} \right) r\,dr\,dx \tag{44}$$

where $\vec{f}_m = f_{x_m}\vec{e}_x + f_{r_m}\vec{e}_r + f_{\theta_m}\vec{e}_\theta$ and $\{F_{x_m}\}$, $\{F_{\theta_m}\}$, and $\{Q_m\}$ are vectors of the nodal values of f_{x_m}, f_{θ_m}, and q_m. The force component f_{r_m} is set equal to zero since it is small compared to the other force components of a propeller.

A dipole located at the point r_d, x_d, θ_d is constructed by placing point sources with strengths of opposite sign at $(r_d, x_d + \epsilon, \theta_d)$ and $(r_d, x_d - \epsilon, \theta_d)$. For a point source of strength Q_0 at (r_s, x_s, θ_s), $q = Q_0\delta(r - r_s)\delta(x - x_s)\delta(\theta - \theta_s)$. Representing this by a fourier series in θ gives the coefficients

$$Q_m = \frac{Q_0}{2\pi}\delta(r - r_s)\delta(x - x_s) \tag{45}$$

which are used in Eqs. (43) and (44). The exact solution of this dipole is the superposition of the exact solutions for the two point sources. The nondimensional exact solution of a point source of frequency η_r and strength Q_0 is

$$p_s = \frac{iQ_0\eta_r}{4\pi R_{ps}} \exp(-i\eta_r R_{ps}) \tag{46}$$

where $R_{ps}^2 = (r - r_s)^2 + (x - x_s)^2$.

Table 1 gives value for the H_1 error norms[13] of the exact solution compared to the finite element solution for an off-axis dipole. The dipole is located at $r_d = 0.183811$, $x_d = 0$, $\theta = 0$ with $\epsilon = 0.000163$. These values are nondimensionalized with respect to the acoustic wavelength. The finite element solutions are constructed by solving, individually, the problem of Eqs. (40-44) for the first N modes. Then Eq. (39) is approximated by the finite sum from $-N$ to N with $\theta = 0$. Figure 8 shows contours of constant nondimensional pressure for the Fourier sum of the first 4 modes ($m = -4,4$) at $\theta = 0$. Table 1 indicates that the norm percent error for these plots is less than 0.3%.

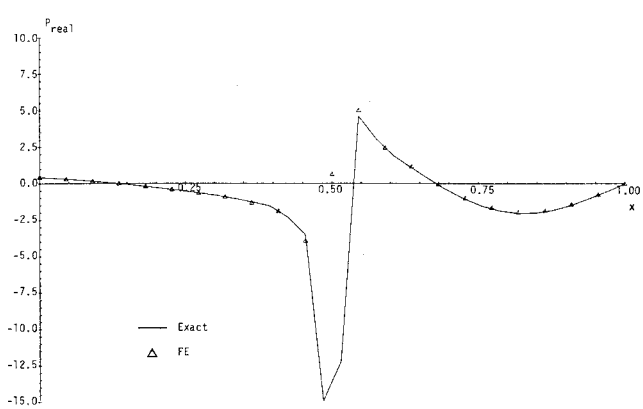

Fig. 6 Real part of acoustic pressure along line $y = 0.50$ for an axial force at $x = 0.50$, $y = 0.50$, $kL = 8.06$, $M = -0.3$. (FE = finite element.)

Table 1 Quasidipole error norms[a] (eight-element-per-wavelength mesh)

N	$\|P_e - P^{(N)}\|_{G^1}$	$\|P_e\|_{G^1}$	$\frac{\|P_e - P^{(N)}\|_{G^1}}{\|P_e\|_{G^1}}$, %
0	0.0006602	0.001025	64.42
1	0.0001484	0.001025	14.48
2	0.0000250	0.001025	2.43
3	0.0000341	0.001025	0.33
4	0.0000022	0.001025	0.21
5	0.0000023	0.001025	0.23

[a]Dipole at propeller tip with point sources separated by 0.004 m. Far-field boundary at 150.6 m 5 × 5 G point integration. Error norms are calculated over the wave envelope region only ($R > 20.6$). $\omega = 174.67$ rad/s, $\rho_0 = 1.225$ kg/m^3, $c_0 = 340.29$ m/s.

Gutin Propeller Theory

In the Gutin propeller theory, the propeller is replaced by a radial distribution of dipoles in the propeller's plane of rotation. The dipoles have axes in the axial and angular directions representing forces in the x and θ directions, respectively. They have strengths related to the local propeller blade loading. This theory has no mechanism for including the effects due to blade thickness, and the chordwise blade loading is considered constant. This theory is a forerunner of current propeller noise prediction techniques, however, it provides a useful model against which to compare a finite element representation.

The force that a propeller with N_p blades exerts on the air at a point (r,θ,z) at a t can be written as

$$\vec{f}_a(r,\theta,x,t) = \sum_{j=0}^{N_p-1} \vec{f}_{sp}(r)\delta(x)$$

$$\times \{u[\theta-\theta_{TE}(r)-2\pi(\Omega t+j/N_p)]$$

$$-u[\theta-\theta_{LE}(r)-2\pi(\Omega t+j/N_p)]\} \quad (47)$$

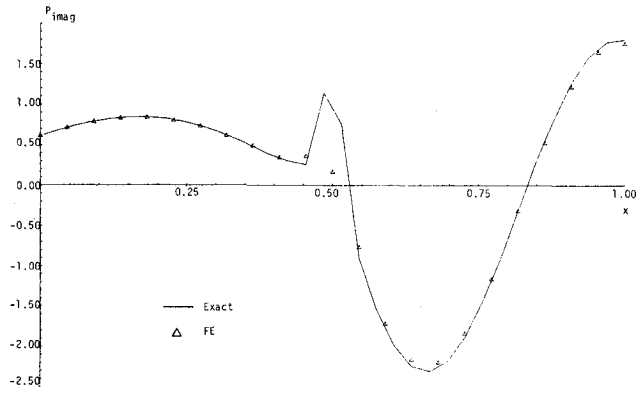

Fig. 7 Imaginary part of acoustic pressure along line $y=0.50$ for an axial force at $x=0.50$, $y=0.50$, $kL=8.06$, $M=-0.3$. (FE = finite element.)

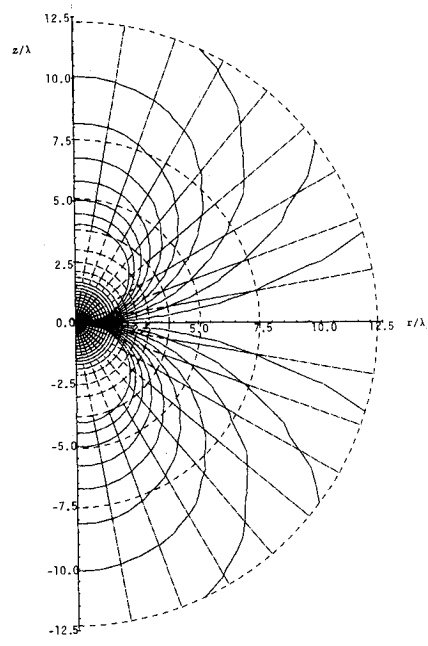

Fig. 8 Contours of equal pressure amplitude for an off-axis dipole, summation of modes $m=-N,N$.

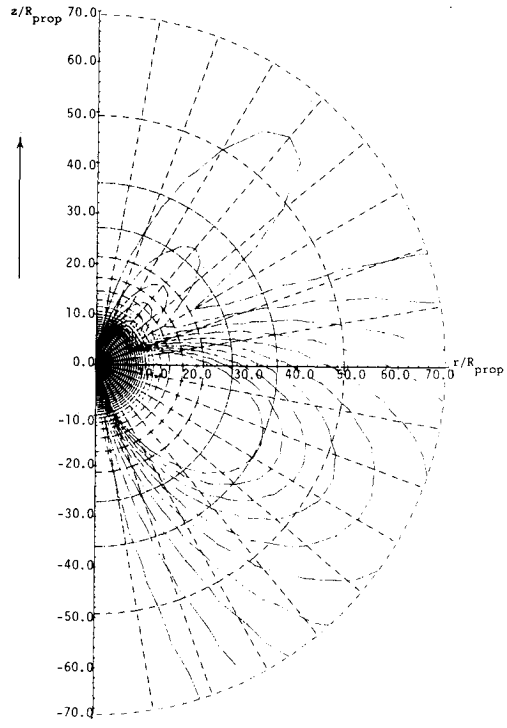

Fig. 9 Contours of equal pressure amplitude for the first harmonic of a two-bladed propeller.

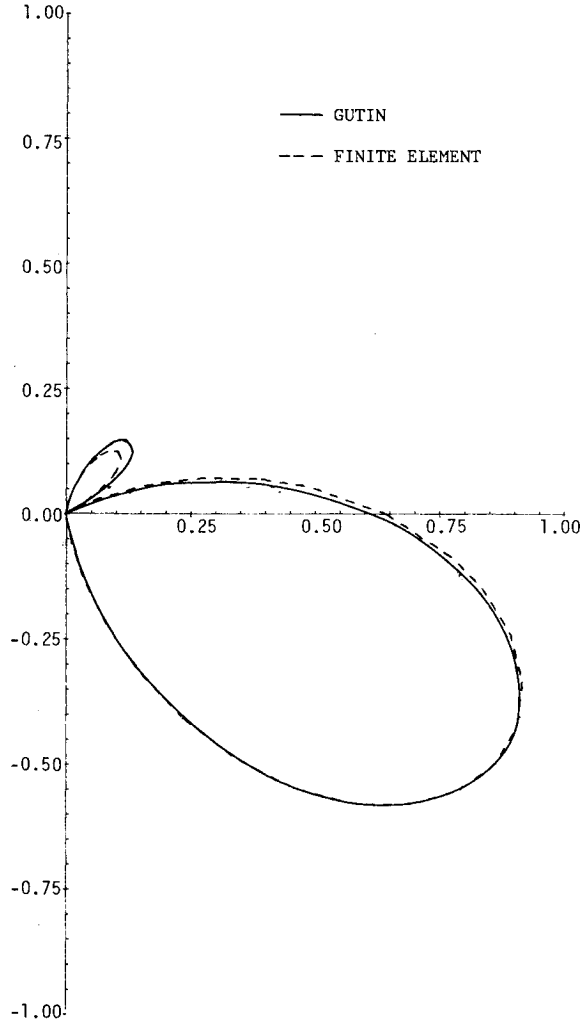

Fig. 10 Polar plot of directivity of the fundamental mode of a two-bladed propeller.

where u is the unit step function, Ω the propeller rotation speed in revolutions per second, and $\theta_{LE}(r)$ and $\theta_{TE}(r)$ equations of the curves formed by projecting the leading and trailing edges of the propeller onto the x = 0 plane. $\vec{f}_{sp}$ is the spanwise loading of the propeller blade, as a force per unit volume exerted on the air by the propeller. Assuming that $\theta_{TE}(r) \simeq \theta_{LE}(r)$, and expressing the force of Eq. (47) as a Fourier series in θ, gives

$$\vec{f}_a(r,\theta,x,t) = \sum_{\ell=-\infty}^{\infty} \vec{F}_m \exp(-im\theta)\exp(i\omega_\ell t) \qquad (48)$$

where $\omega_\ell = m2\pi\Omega$, $m = \ell N_p$, and

$$\vec{F}_m = \delta(z)N_p/(m\pi)\vec{f}_{sp}(r)\sin[m\theta_{LE}(r)] \qquad (49)$$

The forces are now in the form of Eq. (39). $\vec{F}_m$ are the force per unit volume Fourier coefficients used in Eqs. (43) and (44) and $q = 0$. The component in the r direction is also assumed to be zero as a propeller exerts little force on the air in the radial direction. As in the one- and two-dimensional cases, the finite element approximation introduces the Dirac delta of Eq. (49) in only an approximate form, as the continuous function generated by the shape functions.

This type of modeling procedure, implemented for a specific propeller, is compared with the Gutin theory in the far field on the basis of directivity. Figure 9 shows a typical plot of contours of equal pressure magnitudes, and Fig. 10 shows a comparison of far-field directivity. The "exact" results are computed from the Gutin theory. The results shown are for the fundamental mode of a two-bladed propeller with a radius of 2.25 m. The comparison is generally quite good with regard to both directivity and amplitude. The finite element calculations seem to underestimate the minor lobe and slightly overestimate the major lobe near 90 deg. These results are encouraging not only because of the successful comparison but because of the ease with which the theory extends to the representation of both spanwise and chordwise loading and even to multiple blade rows.

Conclusions

It has been shown that acoustic volumetric sources and volumetric forces can be successfully modeled in one, two, and cylindrically symmetric three-dimensional geometries. Volumetric force distributions characteristic of propeller noise sources have also been successfully represented. The main strength of this modeling method is that it is by no means limited to the simple cases described herein, nor to the relatively simple geometry and flow conditions characteristic of most theories presently in existence. This allows the extension of the above work to investigate acoustic sources, such as propellers, with nearby boundaries. This includes propellers in wind tunnels, shrouded props, and ducted fans. It also allows the modeling of the effect of spanwise and chordwise loading distributions on propeller blades with complex shapes.

References

[1]Astley, R.J. and Eversman, W., "A Finite Element Method for Transmission in Nonuniform Ducts without Flow: Comparison with the Method of Weighted Residuals," *Journal of Sound and Vibration,* Vol. 57, No. 3, 1978, pp. 367-388.

[2]Astley, R.J. and Eversman, W., "Acoustic Transmission in Nonuniform Ducts with Mean Flow, Prat II: The Finite Element Method," *Journal of Sound and Vibration*, Vol. 74, No. 1, 1981, pp. 103-121.

[3]Astley, R.J. and Eversman, W., "Wave envelope and Infinite Element Schemes for Fan Noise Radiation from Turbofan Inset," AIAA Paper 83-0709, 1983.

[4]Eversman, W., Parrett, A.V., Preisser, J.S., and Silcox, R.J., "Contributions to the Finite Element Solution of the Fan Noise Radiation Problem," 1984 ASME Paper to be presented at Winter Annual Meeting, Nov. 1984.

[5]Preisser, J.S., Silcox, R.J., Eversman, W., and Parrett, A.V., "A Flight Study of Tone Radiation Patterns Generated by Inlet Rods in a Small Turbofan Engine," AIAA Paper 84-0499, 1984.

[6]Astley, R.J., Eversman, W., and Walkington, N.J., "Accuracy and Stability of Finite Element Schemes for the Duct Transmission Problem," AIAA Paper 81-2015, 1981.

[7]Astley, R.J. and Eversman, W., "Finite Element Formulations for Acoustical Radiation," *Journal of Sound and Vibration*, Vol. 88, No. 1, pp. 47-64.

[8]Irons, B.M., "A Frontal Solution Program for Finite Element Analysis," *International Journal for Numerical Methods in Engineering,* Vol. 2, 1970, pp. 5-32.

[9]Gutin, L., "On the Sound Field of a Rotating Propeller," NACA TM 1195, 1948 (Originally in Russian, 1936).

[10]Farassat, F., "Theory of Noise Generation from Moving Bodies with an Application to Helicopter Rotors," NASA TR R-451, 1975.

[11]Hanson, D. B., "Near Field Frequency Domain Theory for Propeller Noise," AIAA Paper 83-0688, 1983.

[12]Clark, T.L., Ganz, U.W., Graf, G.A., and Westfall, J.S., "Analytic Models of Ducted Turbomachinery Tone Noise Sources. Volume I: Analysis," Boeing Commercial Airplane Co., Rept. D6-43296-1, 1974.

[13]Becker, E.B., Carey, G.F., and Oden, J.T., *Finite Elements: An Introduction*, Vols, I and II (Vol. II by G.F. Carey and J.T. Oden), Prentice-Hall, Englewood Cliffs, NJ, 1981.

[14]Zienkiewicz, O.C., *The Finite Element Method,* 3rd Ed., McGraw-Hill Book Co., New York, 1977.

[15]Norrie, D.H. and deVries, G., *An Introduction to Finite Element Analysis,* Academic Press, New York, 1978.

[16]Eversman, W., "Energy Flow Criteria for Acoustic Propagation in Ducts with Flow," *Journal of the Acoustical Society of America,* Vol. 49, No. 6, Pt. 1, 1970, pp. 1717-1721.